Mechanical Systems and Signal Processing 195 (2023) 110288

Contents lists available at ScienceDirect

Mechanical Systems and Signal Processing

journal homepage: www.elsevier.com/locate/ymssp

Multifidelity data augmentation for data driven passive impact location and force estimation in composite structures under simulated environmental and operational conditions

Aldyandra Hami Seno [a,b], M.H. Ferri Aliabadi [a,*]

[a] Department of Aeronautics, Imperial College London, Exhibition Road, South Kensington, London SW7 2AZ, United Kingdom
[b] Brunel Composites Centre, Brunel University London, Granta Park, Great Abington, Cambridge CB21 6AL, United Kingdom

ARTICLE INFO

Communicated by Spilios Fassois

Keywords:
Composite materials
Impact location estimation
Impact force estimation
Environmental conditions
Operational conditions
Structural health monitoring
Uncertainty quantification
Bayesian updating
Kriging

ABSTRACT

Data driven methods for impact location and severity estimation have great potential for real life application due to their ability to construct meta models that are not affected by changes in structural complexity (e.g. stiffeners and cut-outs). However, to do so, an initial reference database containing known input and output pairs is required to form an accurate meta model. The requirement to collect this data (mainly in the form of experimental tests) is considered by many to be not feasible and hinders the application of data driven methods in large scale, real life structures. Here a new multifidelity approach is presented to reduce the "cost" of constructing the reference database necessary for data driven impact location and severity estimation methods. The proposed cokriging approach is used to combined "cheap" low fidelity FE (Finite Element) simulation data with a limited amount of accurate but "expensive" experimental data to construct a reference database that requires less experimental data sampling (thus lower "cost") but with similar levels of accuracy compared to reference databases that were constructed from pure experimental data. Using previously developed impact location (kriging based localisation) and maximum force estimation (maximum impact force gradient method) methods, the effect of different reference databases with varying amounts of experimental data samples are tested. The results obtained on a CFRP (Carbon Fibre Reinforced Plastic) coupon and stiffened panel showed that using pure FE data for the reference database yielded poor results. By adding a limited number of experimental points, it was shown that the accuracy increases significantly approaching levels achieved using pure experimental data with significantly less samples. The wider context of data fusion is also explored, highlighting the possibility to combine various sources of data (including inspection history as well as data from sister assets) which can possibly be used to create a data driven framework that requires less initial data whilst also being robust and self-improving.

1. Introduction

Composite structures are susceptible to Impact Damage which are not visible and hence difficult to detect without complex inspection methods (e.g. ultrasound) [1,2]. This difficulty has led to interest in developing impact monitoring systems to automatically

* Corresponding author.
E-mail address: m.h.aliabadi@imperial.ac.uk (M.H. Ferri Aliabadi).

https://doi.org/10.1016/j.ymssp.2023.110288
Received 16 September 2022; Received in revised form 8 February 2023; Accepted 11 March 2023
Available online 20 March 2023

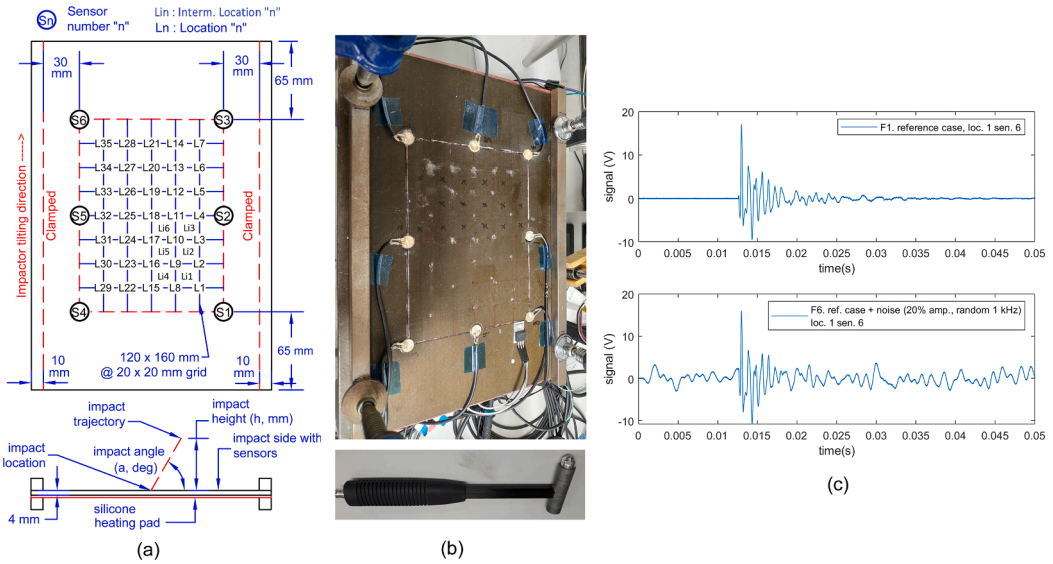

Fig. 1. Flat panel specimen used for collecting experimental impact data: (a) layout of impact and sensor locations, (b) photo of flat panel and impact hammer, (c) example of signals recorded from the reference case (F1) and with artificial noise (F5).

detect severe impact events and reduce inspection requirements [3,4]. To this end, several methods have been developed to estimate the location and severity of an impact event using signals from sensors that are mounted to the structure [5–14].

One of the most popular methods is to capture measurements of lamb waves generated by impact events using Piezo ceramic sensors (PZT) or accelerometers. This approach is referred to as passive sensing, since the lamb wave is not directly generated by the transducers[6,7,12,13]. Lamb waves tend to propagate long distances in thin structures (e.g. airframe) and carry encoded information within their features (e.g. Time of Arrival, amplitude) related to the location and severity of impacts [6,7,13,14]. Different methods have been developed to harness this information and produce reliable and accurate estimates of the impact characteristics. They can be categorised into: wave propagation physics based [9,11,12,15,16] and data driven meta models [5–8,13,17–19].

Wave physics based methods take advantage of the known mechanics of lamb wave propagation in a structure to locate and estimate the severity of impacts [9,11,12,15,16]. One of the most basic methods in this category is the triangulation method, which uses the difference of wave Time of Arrival (ToA) at sensors spread across the structure to estimate the distance of the impact event from these sensors based on the known wave propagation velocity [20]. These class of methods however, are difficult to scale up from simple specimens/coupons to more complex structural components, as it increases the complexity of the wave propagation behaviour. An example is the phenomena of wave refraction that alters the propagation path when the wave passes regions with different properties (e.g. passing through stiffeners, doublers) [10,11] which complicates the wave propagation behaviour.

On the other hand, data driven methods do not take into account the behaviour of the wave propagation and for the most part just form a meta model (e.g. neural networks, pattern matching models) that connects certain inputs (in this case lamb wave features) to certain outputs (in this case the impact location and severity) [7,10,18,19]. Because of this, these models are not affected by the change in complexity of a structure, as long as there is still correlation between the input and output variables [7,10,18,19]. They have been demonstrated to work in complex structures (e.g. stiffened structures or structures with cut-outs that obscure direct propagation paths) with little to no change in general application compared to simple coupons [7,10,18,19]. Thus these methods, due to their adaptability, have potential for deployment in structures in real life, which may contain various sources of complexity [7,10,18,19].

However, as these methods do not take into account the wave propagation behaviour, the only way they are able to form a meta model to connect an input and output is to provide a reference database or train the algorithm with an initial known set of input and output data pairs [5,7,10,19]. This is considered by many as the Achille's heel of data driven methods which prevents them from being used in real life, as collecting initial data for large structures, as well as including all possible variations caused by operational and environmental conditions, results in an unfeasible amount of initial data required [5,7,21].

Data driven methods for impact location and maximum force estimation that are robust towards variations caused by simulated environmental and operational conditions have been developed in previous studies [5–7,21], thus these factors need not be included in the reference database. This reduces the amount of initial data points required to just the spatial sampling along the structure [5–7], which as mentioned before will be a problem for large structures (e.g. an entire aircraft).

Previous studies have demonstrated that Finite Element (FE) models can generate simulated lamb waves with features that can be used to estimate the location and severity of simulated impacts, similar to what is done with experimental data [18,19]. However, no attempt has been made to see whether simulated lamb waves are good enough to substitute actual experimental data samples for use in estimating the location and severity of an actual impact on a real structure.

There are various sources of variation and uncertainty that may not be captured in an FE model [15,22–24]. Thus, rather than including all these factors and increasing the complexity of an FE model, a multifidelity approach using cokriging is presented to

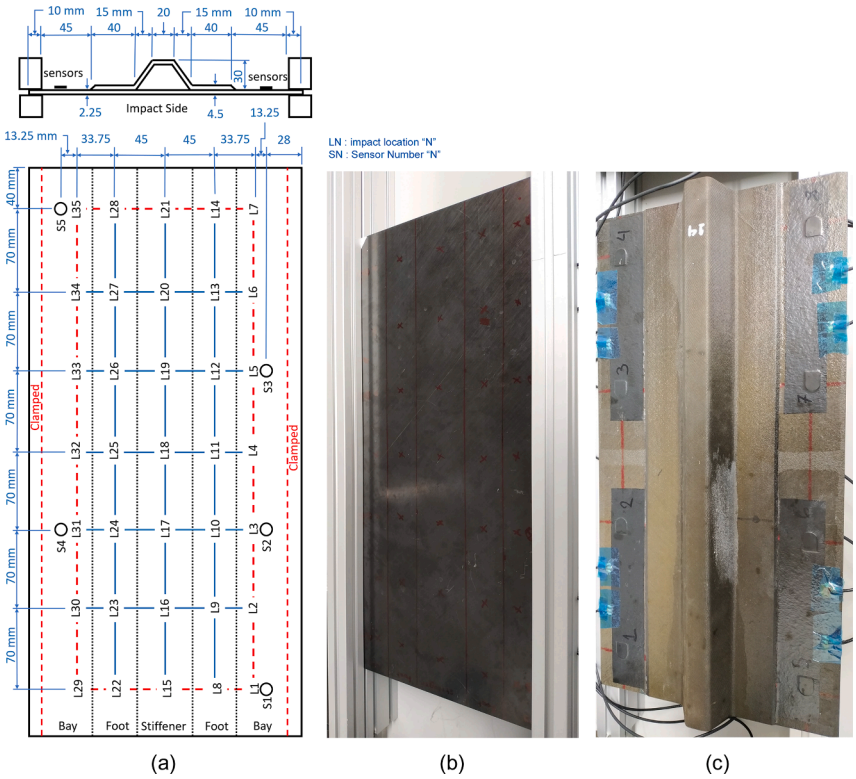

Fig. 2. Stiffened composite panel specimen for collecting experimental impact data: (a) layout of impact and sensor locations, (b) photo of specimen impact side, (b) photo of bottom side with stiffener.

combine a "cheaper" but less accurate (lower fidelity) data source (FE models) with more "expensive" but more accurate (higher fidelity) data (experimental sampling) using the correlation of the data in the 2 datasets is proposed [25–27]. The aim is to generate as much data using the "cheaper" source to gain spatial coverage and then to calibrate it using the least amount of "expensive" experimental data. This reduces the "cost" of constructing a reference database for data driven methods, thus making them more feasible for real life application. Here we, take advantage of both datasets to obtain a cheaper yet more accurate final database than can be achieved by each dataset alone.

In this study a comparison of the performance of impact location and maximum force estimation under simulated environmental and operational conditions with previously developed methods is conducted for different reference databases: purely experimental samples, purely FE samples and a multifdelity combination of FE and experimental samples. The purpose is to observe how the multifidelity approach can create a right balance between reduced number of experimental data sampling needed and FE simulations while maintaining a reasonable level of accuracy.

2. Experimental setup

The experimental impact data (for use as the high fidelity data set) was collected from 2 carbon fibre composite specimens: a flat panel (M21 T800s prepreg, [0/+45/-45/90/0/+45/-45/90]s layup, Fig. 1) and a more complex stiffened panel (M21 T800s prepreg, [45/-45/0/0/90/0]s layup, Fig. 2). The flat panel has a silicone heating mat underneath with a temperature control unit to simulate elevated temperatures. Each Panel has 8 PZT sensors attached, however not all were used due to limitations of measurement channels. Only 6 sensors were used for the flat panel and 5 on the stiffened panel (not 6, due to sensor damage from previous testing campaigns) as shown in the layout in Fig. 1a and Fig. 2a, respectively.

Impacts with random energies and angle were generated and recorded with a PCB Piezotronics 086C03 instrumented hammer (Fig. 1b). The hammer has space for a 100 g attachment to simulate impacts of varying mass. The hammer tip was interchangeable with 2 materials available, plastic and steel, to simulate impacts from different stiffness materials.

The signals were recorded from PZT sensors on each panel via 10x attenuation oscilloscope probes attached to an NI PXI-5105 8 channel oscilloscope. Signals were recorded at 2 MS/s and with a length of 100,000 samples. One channel of the oscilloscope was used to measure the impact force from the hammer.

Impact data was collected from the locations laid out in Fig. 1a and Fig. 2a for cases described in Table 1 with four repetitions for each location. For the flat panel, these cases represent parametric changes (case F2 – F6) from a reference case (F1) and simulate the common environmental and operational conditions encountered in operation [5–7]. To simulate vibration noise (case F5), artificial 1

Table 1
Experimental impact cases collected on flat and stiffened panel.

ID	Case	Parameters	Number of Impacts
Flat Panel			
F1	Reference case	Tip: steel, Temp.: 24 °C, mass: hammer only	140 (35 loc. × 4 rep.)
F2	Increased mass	Tip: steel, Temp.: 24 °C, mass: added 100 g	140 (35 loc. × 4 rep.)
F3	Increased temp.	Tip: steel, Temp.: 70 °C, mass: hammer only	140 (35 loc. × 4 rep.)
F4	Plastic tip	Tip: plastic, Temp.: 24 °C, mass: hammer only	140 (35 loc. × 4 rep.)
F5	Reference + noise	Tip: steel, Temp.: 24 °C, mass: hammer only	140 (35 loc. × 4 rep.)
F6	Intermediate locs.	Tip: steel, Temp.: 24 °C, mass: hammer only	24 (6 loc. × 4 rep.)
Stiffened Panel			
S1	Reference case	Tip: steel, Temp.: 24 °C, mass: hammer only	140 (35 loc. × 4 rep.)

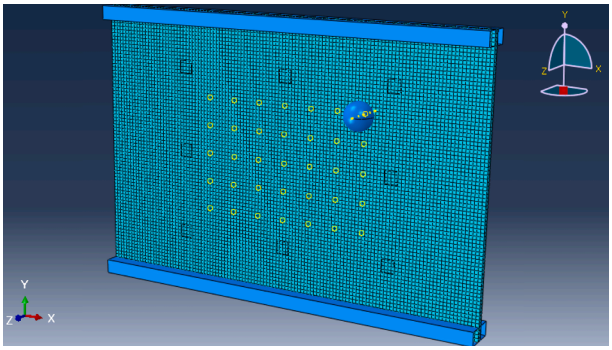

Fig. 3. Finite element model of flat panel showing impactor, sensors and impact locations. Model consists of 5 analytical rigid components (clamps and impactor), 9280 SC8R continuum shell elements (panel) and 8 M3D4R membrane elements (sensors) with a total of 18986 nodes.

Table 2
Material properties used in finite element model.

Property	Value	Property	Value
M21 T800S Prepreg (lamina model) [28,29]		Piezo ceramic (PIC 255, isotropic) [30]	
Longitudinal stiffness, E_{11} (MPa)	171000	Stiffness, E (MPa)	62100
Transverse stiffness, E_{22} (MPa)	11470	Poisson's ratio, υ	0.34
Shear Modulus, G_{12} (MPa) & G_{13} (MPa)	4830	Density, ρ (tonne/mm^3)	7.8e-9
Shear Modulus, G_{23} (MPa)	3720	Piezo. coefficient, d31 (C/N)	0.18e-9
Poisson's ratio, υ_{12}	0.35	Permittivity, ε (F/m)	14.6e-9
Density, ρ (tonne/mm^3)	1.6e-9	Contact/interaction	
Mass damping coefficient, α (calibrated)	500	Contact stiffness, k (calibrated)	500
		Friction coefficient	0.3

kHz random noise was generated through lowpass filtering of white noise and then scaled to 20% of the maximum absolute amplitude of the signals in the reference case (F1).

3. Finite element modelling of impacts

Finite Elements (FE) modelling was conducted as a source of low fidelity data. The target of the simulation was to be as "cheap" as possible whilst achieving the best possible correlation with experimental data. Next, the simulation and calibration of the FE model is discussed.

3.1. Finite element model

To simulate impacts and the induced lamb waves, ABAQUS commercial FE software with explicit solver was used. The flat panel was modelled as a solid and was meshed with continuum shell elements (Fig. 3). The material was modelled as a composite layup following the stacking sequence mentioned in section 2 using the property values shown in Table 2 [28,29]. As the flat panel had a silicone heating mat attached underneath, a uniformly spread non-structural mass of 213 g (obtained from weighing the panel minus the weight from the density of the material) was added to the panel model. The PZT sensors were modelled as single rectangular membrane elements (8.86 mm × 8.86 mm × 1 mm, equivalent area as the 10 mm diameter circular sensors used) and attached to the panel surface with tie constraints (Fig. 3) to match nodal displacements. The thickness (t) was defined in the section of the membrane.

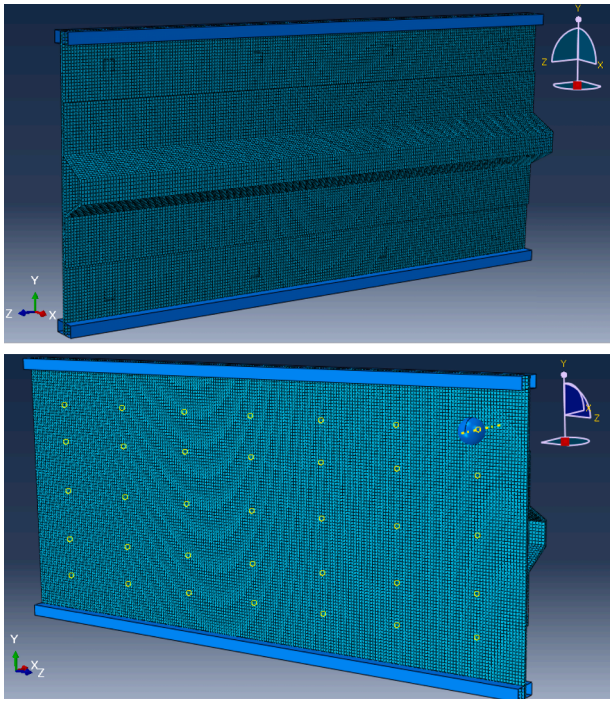

Fig. 4. Finite element model of stiffened panel: (top) bottom side with stiffener and sensors, (bottom) top side with impactor and impact locations. Model consists of 5 analytical rigid components (clamps and impactor), 32400 SC8R continuum shell elements (panel) and 8 M3D4R membrane elements (sensors) with a total of 65944 nodes.

The isotropic PZT sensor properties are given in Table 2 [30]. The clamps were modelled as analytical rigid surfaces and placed in contact with the panel surface and given full displacement and rotation constraints to hold the panel in place through contact and friction (Fig. 3).

The same approach was followed for the stiffened panel (Fig. 4), with the difference that the panel consisted of 2 solids, the base and the stiffener. Both were meshed with continuum shell elements and coupled through tie constraints. The base plate and stiffener were given the same stacking sequence following what was mentioned in section 2, with all material property values listed in Table 2.

As previously mentioned in section 2 the main source of experimental data were hammer impacts. This was done as it was a quick and simple way of obtaining experimental data points with measured force and is most likely what experimental data sampling on actual structures in operation would look like. However, these impacts are difficult to model as they are random due to the nature of handheld actuation. In this case however, the main features that are used in the impact location and maximum force estimation (Time of Arrival and maximum force gradient [5–7]) later on (section 6) are independent of impact case (impactor mass, angle, energy, etc.), and as such it does not matter whether the modelled impact case does not match that of the experiments.

Because of that, here the choice of impactor model design was based on simplicity and also for calibration purposes to find missing parameter information (contact stiffness and mass damping coefficient, see Table 2) later on in section 3.2. An analytical rigid sphere surface (20 mm diameter) was defined to simulate an impactor (Fig. 3 and Fig. 4) and was given a lump mass of 100 g at the reference point in the centre. Displacement and rotation constraints were also applied at the reference point to prevent any movement except for translation transverse to the panel surface. The impactor was situated on the impact side of each panel at a distance of 0.01 mm from the surface to simulate the moment prior to contact. An initial velocity of 0.707 m/s was given to simulate impacts of 50 mJ energy. The impactor was moved to whichever location it was needed to simulate impacts, following the laid out locations (same as the experimental tests) in Fig. 1a and Fig. 2a, respectively resulting in 35×1 impacts.

Contact was defined through the general contact option for all contacts between components (panel, clamps and impactor) with a friction coefficient of 0.3 and a linear pressure-overclosure contact behaviour [31]. Two vital parameters that were not readily available from literature were the contact stiffness and damping coefficient (Table 2), both which were obtained through calibration using experimental data on a coupon level (the flat panel) as will be explained in the next section.

The output of the FE model was the acceleration of the impactor at the reference point and the principal strain components of the membrane elements of each sensor, all of which were sampled at 2 MS/s. The simulation itself was run for 20 ms from start of impact to collect a reasonable duration of measurements (1063.5 ± 53.3 s and 4109.25 ± 234.8 s average CPU time for each impact simulation for flat and stiffened panels using Intel i7-6500U @2.5 GHz, 4 core CPU). The impact force history was obtained by multiplying the acceleration with the mass of the impactor. The signal voltage (V) from the sensors were obtained from the principal strain components (ε_{11}, ε_{22}) using the PZT sensor properties in Table 2 and equation (1) below [32].

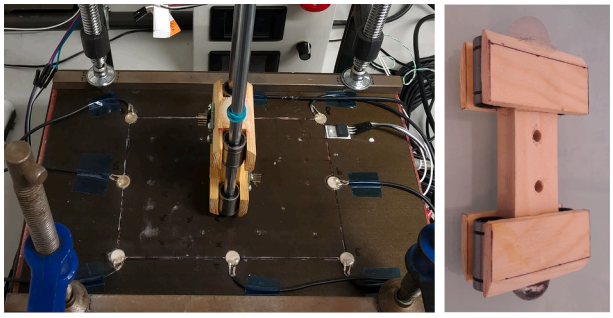

Fig. 5. Drop impactor used to collect experimental data on the flat panel for finite element model calibration: setup (a) and impactor (b).

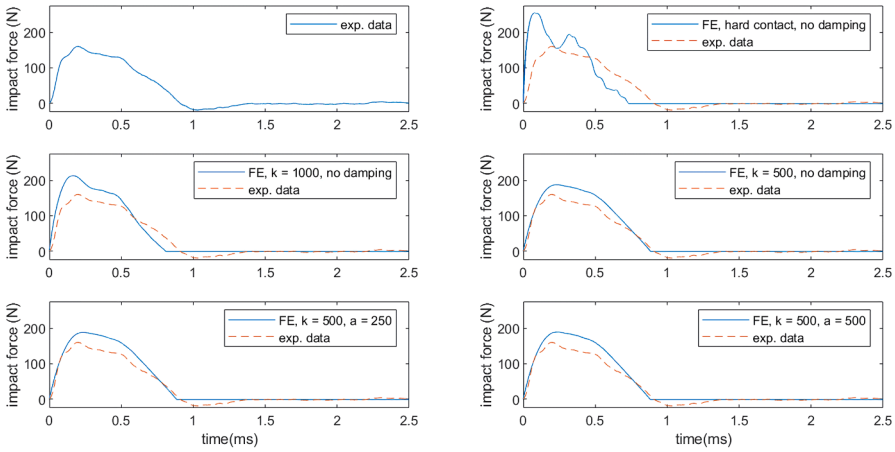

Fig. 6. Experimental drop impact force history and finite element results with various values of contact stiffness (k) and damping coefficient (α).

$$V = \frac{Ed_{31}t}{\varepsilon}(1-\upsilon)(\varepsilon_{11}+\varepsilon_{22}) \tag{1}$$

3.2. Finite element model calibration

To obtain the material property values for contact stiffness and damping coefficient (Table 2), calibration was done using experimental data gathered from 1 impact on the flat panel using a controlled drop impactor as shown in Fig. 5. Since the flat and stiffened panel are of the same material, the calibration results on the flat panel can also be applied on the stiffened panel. Thus, here we demonstrated FE model calibration on the coupon level, which was then used for more complex structures (in this case the stiffened panel).

The impactor (Fig. 5b) has a steel 20 mm diameter spherical tip, a total mass of 100 g, and was dropped from a height of 50 mm to produce an impact of 50 mJ energy as is simulated in the FE model. As the impactor has no force measurement system, the impact force history was obtained from deconvolution of measured signals as was done in a previous study [6]. To do so, first the actual force (F) and measured signal (S) spectral components from the hammer impact (F1) at the target location (here it was calibrated from location 1, Fig. 1a) were used to obtain the spectral transfer function (TF = F/S). Afterwards, the obtained transfer function was used to obtain the impact force history spectral components (F_{drop} = TF S_{drop}) from the drop impact signal spectral components (S_{drop}). Finally, the drop impact force history was obtained by inverse Fourier transform of the obtained force spectral components. As there are 6 sensors, 6 impact force histories were produced, all of which were averaged to obtain the final impact force history (Fig. 6).

As both the impactor (analytical rigid) and plate (continuum shell) are rigid in the transverse direction, the interaction between impactor and plate during contact needs to be modelled [19]. Here, a linear contact stiffness (k) approach is used to define the relation between the transverse displacement of the contact area and the contact pressure. As the value of k is not readily available in literature for the materials used, calibration is done to find the appropriate value of k using the experimental sample as the reference. Fig. 6 shows the effect of different contact stiffness values on the impact force history. It can be seen that with a completely "hard" impact where the stiffness is infinite, the impact force was overestimated. Lowering the contact stiffness reduced the impact force until it became close to the experimental data at a stiffness value of k = 500 (Fig. 6).

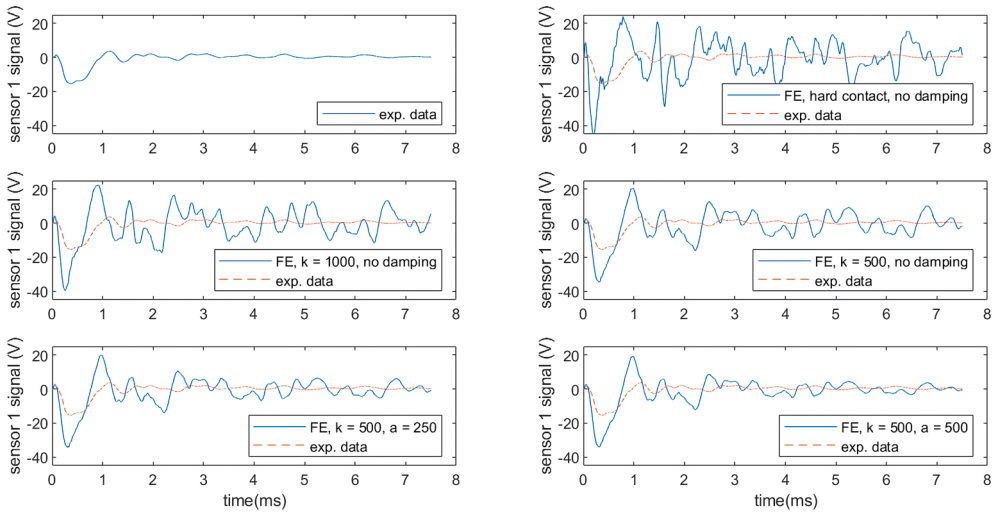

Fig. 7. Experimental drop impact signal from sensor 1 and finite element results with various values of contact stiffness (k) and damping coefficient (α).

In the experimental signal (Fig. 7), it can be seen that after the initial forced response [6], the residual free vibrations attenuate rapidly. On the other hand, the signal from the "hard" FE model showed very low attenuation of the free vibration. Using a lower contact stiffness introduced some slight attenuation, but not as much as the experimental signal. Thus, here mass proportional Rayleigh damping (α) [31] was added to damp the low frequency (based on natural frequencies of the structure [6]) free vibrations. From Fig. 7, increasing the damping coefficient (α) increases the attenuation of the signal, until at a coefficient value of 500 it approaches the level seen in the experimental signal. Although the amplitude of the signal itself differs between FE and experimental data, this will be rectified by the multifidelity approach later on in section 5. The obtained values for contact stiffness and damping coefficient were then used for all FE simulations.

4. Signal feature extraction for impact location and maximum force estimation

Here, the data driven impact location (kriging based localisation [33]) and maximum force estimation (maximum impact force gradient method [6]) methods developed in previous studies were used (will be described later on in section 6). One impact from each location in the experimental reference case of both panels (hammer impacts in case F1 and S1) was taken to form the high fidelity reference database of these algorithms whilst the rest of the experimental data (hammer impacts outlined in Table 1) were used as test cases. The FE signals were used to form a lower fidelity reference database. Specific features were then extracted from the experimental and FE signals to be used as inputs for the impact location and maximum force estimation algorithms.

For impact localisation, the signal Time of Arrival (ToA) was used as the input feature and was extracted using the NSET (Normalised Smooth Envelope Threshold) method [7]. To mitigate vibration noise (case F5), the signals were first highpass filtered using a 2 kHz IIR Butterworth filter. Afterwards, the signals were rectified and then lowpass filtered to generate the NSET envelope using a 250 Hz IIR Butterworth lowpass filter. Finally, the signals were normalised using the maximum absolute amplitude from the set of sensors. The ToA was taken as the time when the envelope surpasses a threshold value of 0.05. As the actual time of impact is unknown, the ToA is defined in the form of the difference between signal arrivals from the first arriving signal in the set of sensors [7].

For the maximum impact force estimation, the maximum absolute amplitude (A_{MA}) of the measured signals (without any signal processing) were used as the input feature [6]. As the maximum impact force estimation requires the knowledge of the maximum impact force gradients (G_{MA}) beforehand [6], the measured force from impacts used for the reference database (case F1 and S1) were combined with the subsequent maximum absolute amplitude (A_{MA}) to calculate the gradients.

The final test database consisted of the ToA and A_{MA} of each sensors for all test impacts, whilst the reference database (both high and low fidelity) consisted of ToA and G_{MA} (to be used with the A_{MA} from the test databases) of each sensors for the selected impacts [5,6,33]. The high and low fidelity reference databases were then the subject of the proposed multifidelity approach as elaborated in section 5.

5. Multifidelity reference database augmentation using cokriging

Cokriging works by looking at the spatial correlation between data points in multiple datasets (e.g. z, v), to interpolate a data point that is a member of one of the datasets (z) at a point/location using a weighted linear combination of all the data points in the known datasets (z, v) [25]. Having additional datasets (v) that are more densely sampled than the dataset to be interpolated (z), gives better interpolation than using a single dataset (e.g. ordinary kriging) as the additional correlated datasets provide more information

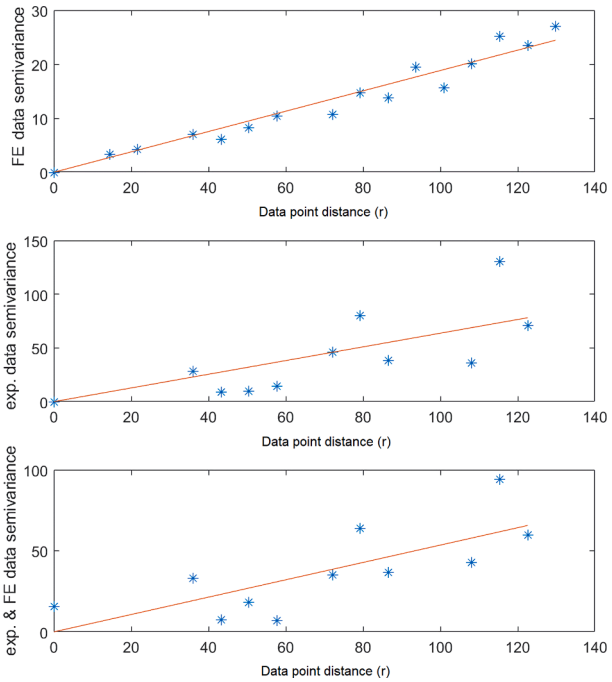

Fig. 8. Semivariance of data points within the reference databases of the flat panel from the finite element (FE) simulations (top), experimental data samples (middle) and combination of both (bottom), including fitted linear functions for each.

regarding the behaviour of the data points in between the known points in the target dataset [25]. This way, cokriging can be used to construct a reference database with just a limited amount of "expensive" experimental high fidelity data (z), aided by "cheap" and more densely sampled low fidelity (v) FE simulations to achieve similar levels of accuracy to a reference database constructed using purely high fidelity data.

The spatial (x,y) correlation between known/reference points are commonly described in the form of semi-variance (γ), as shown in equation (2) [25], which captures how the correlation between data points decreases with increasing distance ($r = \sqrt{x^2 + y^2}$) between them. When looking at the semivariance between data points in the same dataset (e.g. A = B = z), the semivariance was calculated for all possible data point pairs (z_i, z_j, N_r number of points) in the dataset. When looking at the semivariance between datasets (e.g. A ≠ B, A = z, B = v), the semivariance value was calculated between all possible data point pairs at locations that were concurrently sampled for both datasets (z_i, v_j, N_r number of concurrently sampled locations). The semivariance was then averaged by the number of data point pairs that share the same distance (N_h). As data point pairs do not always share uniform distances, the distances are grouped into bins to allow averaging (here 20 bins were used). A linear semivariance function ($\gamma^f[r] = G_\gamma\, r$) was then fitted over the discreet semivariance points to obtain a continuous expression of the semivariance with distance. Fig. 8 shows an example of the semivariance and fitted functions for the G_{MA} of sensor 6 of the flat panel using the experimental data (γ^{zz}), FE (γ^{vv}) data and combination of both (γ^{zv}).

$$\gamma\left(r^{ref}\right) = \frac{1}{2N_h}\sum_{i}^{Nr}\sum_{j}^{Nr}\left(A_i^{ref,r} - B_j^{ref,r}\right)^2 \tag{2}$$

To interpolate a data point at a certain location (x^{in}, y^{in}), first the distances between the known data points (r^{ref}) as well as the distance between the input point to the known data points (r^{in}) were calculated. Using the fitted functions ($\gamma^{zz}[r]$, $\gamma^{vv}[r]$, $\gamma^{zv}[r]$) and distances (r^{in}, r^{ref}), the semivariance values were calculated for the known ($\gamma^{zz}[r^{ref}]$, $\gamma^{vv}[r^{ref}]$, $\gamma^{zv}[r^{ref}]$) data pairs as well as the input and known ($\gamma^{in}[r^{in}]$) data point pairs (Nz number of high fidelity points and Nv number of low fidelity data points). The system of equations (3) [25,34] (I is a vector of 1 s and O is a vector of 0 s) was then solved to obtain the cokriging weights (w^{zz}, w^{zv}) and Lagrange parameters (μ^{zz}, μ^{zv}). The estimated data point (z^{est}) and the associated variance/uncertainty (σ^{est}) were then calculated using equation (4) and (5) [25,34]. As the semivariance always has a positive value, the kriging weights (w^{zz}, w^{zv}) and Lagrange parameters (μ^{zz}, μ^{zv}) solved from equation (3) were constrained to be positive (MATLAB lsqnonneg solver used here) so that the variance always has a real value.

$$\begin{bmatrix} \gamma_{i,j}^{zz}(r^{ref}) & \gamma_{i,l}^{zv}(r^{ref}) & I_{i,1} & O_{i,1} \\ \gamma_{k,j}^{zv}(r^{ref}) & \gamma_{k,l}^{vv}(r^{ref}) & O_{k,1} & I_{k,1} \\ I_{1,j} & O_{1,l} & 0 & 0 \\ O_{1,j} & I_{1,l} & 0 & 0 \end{bmatrix} \begin{bmatrix} w_i^{zz} \\ w_j^{zv} \\ \mu^{zz} \\ \mu^{zv} \end{bmatrix} = \begin{bmatrix} \gamma_i^{in}(r^{in}) \\ \gamma_j^{in}(r^{in}) \\ 1 \\ 0 \end{bmatrix} \begin{matrix} i,j = 1,2,\cdots Nz \\ k,l = 1,2,\cdots Nv \end{matrix} \tag{3}$$

$$z^{est} = \sum_{i=1}^{Nz} w_i^{zz} z_i^{ref} + \sum_{j=1}^{Nv} w_j^{zv} v_j^{ref} \tag{4}$$

$$\sigma^{est} = \sqrt{\mu^{zz} + \sum_{i=1}^{Nz} w_i^{zz} \gamma_i^{in}(r^{in}) + \sum_{i=j}^{Nv} w_i^{zv} \gamma_j^{in}(r^{in})} \tag{5}$$

To build a reference database, interpolation was done for the signal features (ToA and G_{MA}) for all 35 impact locations on the flat and stiffened panel as shown in Fig. 1a and Fig. 2a using a limited number of experimental samples as well as the full FE reference database (35 points). The number of experimental samples was varied starting from 5 (all 4 corners and middle point) all the way up to 35 points (all experimental data) to see the effect on impact localisation and maximum force estimation accuracy. Here, only the estimate value was used in the reference database whilst the variance was used to determine the sampling strategy. When increasing the experimental points from 5 (starting with locations 1,7,18,29,35, Fig. 1a and Fig. 2a) to 35, the selection of which location to sample next was based on the points with the highest variance (if there were multiple points with the same level of variance, then all points were sampled simultaneously) as it shows the area with highest uncertainty. By sampling these locations, it was expected to reduce the uncertainty of the estimated values and give the best spatial coverage.

6. Impact location and maximum force estimation methods

6.1. Kriging based impact localisation method

The kriging based impact localisation method uses similar principles to the cokriging method for reference database interpolation in section 5. It uses kriging, which is the single dataset form of cokriging as the base [25], but instead of interpolating data points based on their location, it uses the "distance" or difference between impact signal features to interpolate characteristics of the impact. For localisation, the characteristics interpolated were the impact location coordinates (x,y), using the ToA as the input feature [33].

Similar to cokriging, first the semivariace (γ^{ToA}) was calculated for the impact location coordinates (x,y) using the difference (L2 norm) in ToA (h^{ref}) for all possible reference database pairs (Nr number of database points) as shown previously in equation (2). Then a linear semivariance function was fitted ($\gamma^{f,ToA}[h] = G_{ToA}\, h$) to the discreet semivariance values. To estimate the location of an incoming impact, the L2 norm of the input ToA (h^{in}) was calculated against the ToA of the reference database points. Using the fitted function and the L2 norm of the reference database points and the input point, the semivariance values ($\gamma^{ToA,in}$) were obtained from the fitted semivariance function. Equation (6) is the single dataset form of equation (3), and was solved (with the same lsqnonneg solver as cokriging in section 5) to obtain the kriging weights (w^{ToA}) and Lagrange parameter (μ^{ToA}). The location estimate (c^{est}) as well as the uncertainty/variance (σc^{est}) was then calculated using equation (7).

$$\begin{bmatrix} \gamma_{ij}^{ToA}\left(h^{ref}\right) & I_{1,i} \\ I_{1,j} & 0 \end{bmatrix} \begin{bmatrix} w_i^{ToA} \\ \mu^{ToA} \end{bmatrix} = \begin{bmatrix} \gamma_i^{ToA,in}\left(h^{in}\right) \\ 1 \end{bmatrix} i,j = 1,2,\cdots Nr \tag{6}$$

$$c^{est} = \sum_{i=1}^{Nr} w_i^{ToA} c_i^{ref} \quad , \quad \sigma c^{est} = \sqrt{\mu^{ToA} + \sum_{i=1}^{Nr} w_i^{ToA} \gamma_i^{ToA,in}\left(h^{in}\right)} \tag{7}$$
$$c = x \text{ or } y \text{ coordinates}$$

Here, the ToA was not used all at once in 1 input vector, rather it was split into multiple smaller input vectors containing permutations of the possible combinations of sensors [5] to obtain a more robust estimation (e.g. permutations of 5 sensors out of 6 gives 12345, 12346, 12,356 and so on). This resulted in multiple final estimates depending on the number of combinations used (a combination of 5 sensors out of 6 for the flat panel and a combination of 4 sensors out of 5 for the stiffened panel was used). To combine the final estimate distributions (constructed with the estimate as mean and uncertainty as standard deviation), Bayesian updating was used, as shown in equation (8) [8,33], with a random initial prior distribution (P[O]) that was updated by the Ne number of estimate distributions (P[N|O]) to obtain an informed final estimate (P[O|N]).

$$P_i(O|N) = \frac{P_i(N|O)\, P_i(O)}{P_i(N)} \qquad P_i(N|O) = P_{i-1}(O|N) \qquad i = 1,2,3\cdots Ne \tag{8}$$

From the resulting distribution, an estimate range was taken using a 95% confidence interval for each coordinate (x,y). An elliptical uncertainty range was then taken around the estimate point using the range for the x and y coordinates as the semimajor axes (x_{sm},y_{sm}), designating the area where there is 95% confidence the real impact was located in [33]. To calculate the error of this range, the Root

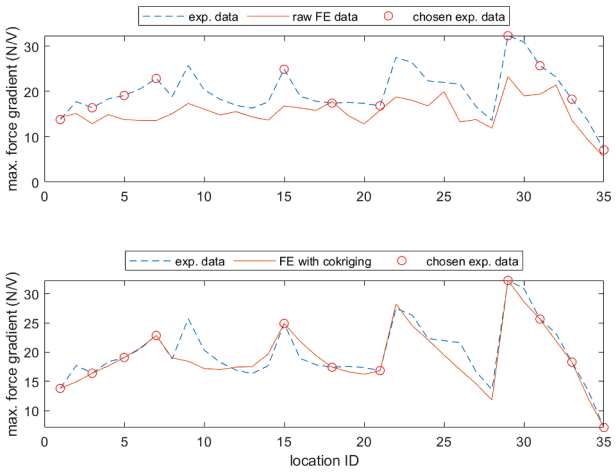

Fig. 9. Comparison between maximum impact force gradient for sensor 6 on the flat panel for: (top) finite element data vs experimental data, (bottom) cokriged finite element data (using 11 experimental data samples) vs experimental data.

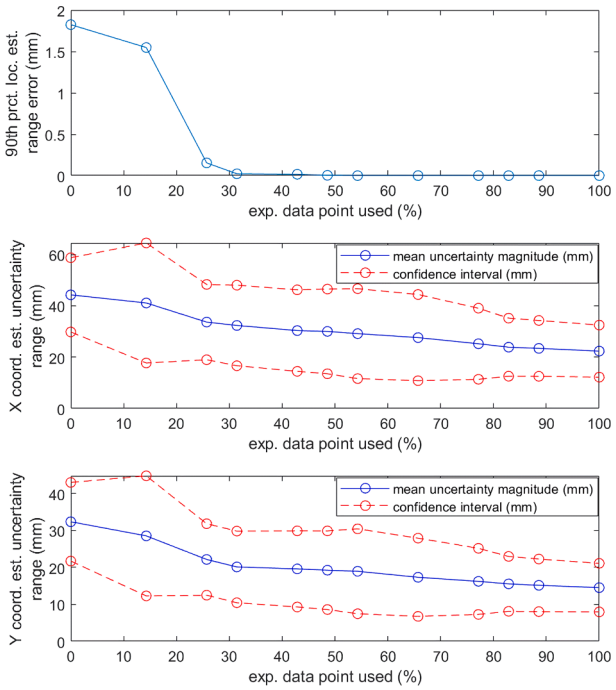

Fig. 10. Change in flat panel impact location estimation error (top) and uncertainty (middle and bottom) as experimental high fidelity data is gradually added to cokrig low fidelity finite element data.

Square Error ($RSE = \sqrt{{x_{err}}^2 + {y_{err}}^2} = \sqrt{(X^{act} - X^{est})^2 + (Y^{act} - Y^{est})^2}$) between the estimated (x^{est},y^{est}) and actual (x^{act},y^{act}) impact location was calculated and then compared with the estimated uncertainty range ($RSE_{lim}[\theta]$) for the angle between the estimate and actual location (θ), as shown in equation (9). If the RSE was smaller than the uncertainty range (thus the actual location is located inside the uncertainty range), the error of the uncertainty range (RSE_{range}) was taken as 0. If not, the uncertainty range error was calculated from the edge of the uncertainty range (RSE_{range} = RSE - RSE_{lim}). To summarise the uncertainty range errors for multiple impacts in each case (Table 1), a gamma distribution was fit to the errors and the 90th percentile of estimation range error (RSE_{R90th}) was used as the summarising metric [5,7,33].

$$RSE_{lim}(\theta) = \frac{x_{sm} y_{sm}}{\sqrt{(y_{sm}\cos[\theta])^2 + (x_{sm}\sin[\theta])^2}}, \quad \sin(\theta) = \frac{y_{err}}{RSE}, \quad \cos(\theta) = \frac{x_{err}}{RSE} \tag{9}$$

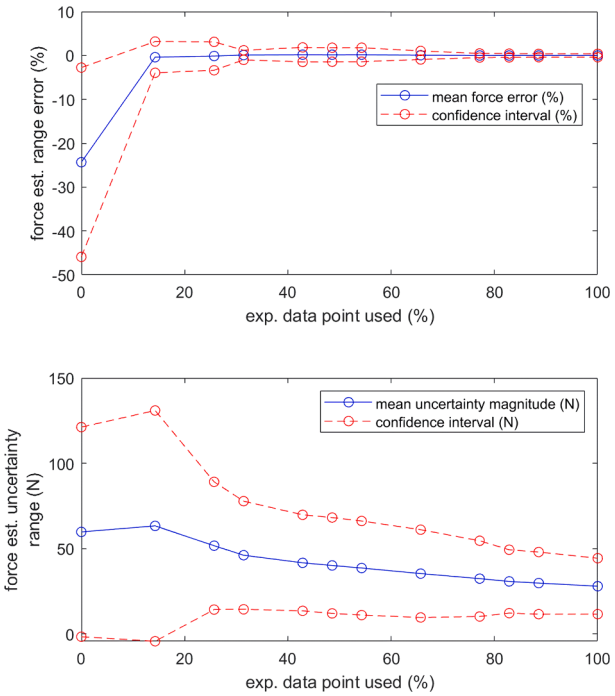

Fig. 11. Change in flat panel maximum impact force estimation error (top) and uncertainty (bottom) as experimental high fidelity data is gradually added to cokrig low fidelity finite element data.

Table 3
Impact location and maximum force estimation for all flat panel cases.

Impact Case		RSE_{R90th} (mm)	RSE_{R90th} (mm)	RSE_{R90th} (mm)	$F_{max,Rerror}$ (%)	$F_{max,Rerror}$ (%)	$F_{max,Rerror}$ (%)
Exp. data usage		0%	31.4%	100%	0%	31.4%	100%
F1	steel hammer, ref case	1.82	0.02	0	-24.3 ± 10.8	0.1 ± 0.6	0.0 ± 0.2
F2	steel hammer, incr. mass	1.28	0	0	-31.9 ± 9.2	-1.2 ± 2.1	-1.3 ± 2.0
F3	steel hammer, incr. temp.	1.02	0.01	0	-20.4 ± 11.8	1.3 ± 2.8	0.8 ± 1.7
F4	plastic hammer	2.03	0.37	0.01	-18.1 ± 11.8	1.9 ± 3.6	1.9 ± 2.5
F5	steel hammer, + noise	1.82	0.02	0	-24.3 ± 10.8	0.1 ± 0.7	0.0 ± 0.6
F6	steel hammer, interm. loc.	0.36	0	0	-25.6 ± 8.6	0 ± 0	0.0 ± 0.3

6.2. Maximum impact force gradient method

Similar to location estimation (section 6.1), the maximum impact force estimation also uses kriging to determine the G_{MA} (estimate and uncertainty) of the incoming impact using the ToA as input [33]. After obtaining the G_{MA} distribution for each sensor, the maximum impact force distribution (F_{max}) was calculated from $F_{max}(x,y) = G_{MA}(x,y)A_{MA}(x,y)(1-\alpha_T[T-T_{ref}])$. For the flat panel, the temperature (T) compensation parameter (α_T = -0.0026, T_{ref} = 24 °C) has been characterised in a previous study [6] and the results were used here (the stiffened panel did not have a different temperature case, thus no need for temperature compensation). As each sensor produces 1 maximum impact force distribution, they were combined together by taking the mean of the distributions [33].

Here, the ToA was also used in combinations as is for localisation, resulting in a maximum impact force distribution for each combination. These distributions were also combined using Bayesian updating to obtain the final maximum impact force distribution. The final estimated maximum impact force range was determined using a 95% confidence interval. If the actual measured impact force ($F_{max,act}$) was within the estimated range, then the maximum impact force estimate range error ($F_{max,Rerror}$) was taken as 0. If not, the estimate range error was calculated from the bounds of the estimate range ($F_{max,range(-)}$ - $F_{max,range(+)}$) as shown in equation (10). Averaging was done to summarise the maximum impact force range errors ($F_{max,Rmean} \pm F_{max,Rstd}$) for each case (Table 1).

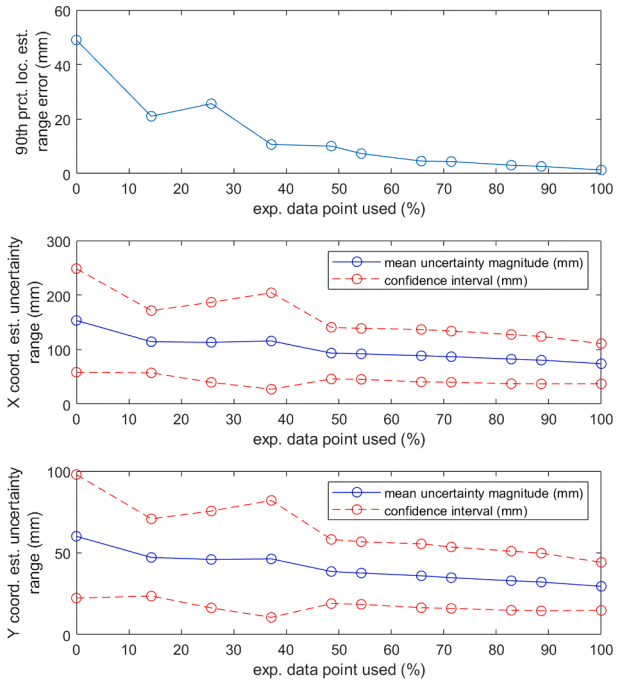

Fig. 12. Change in stiffened panel impact location estimation error (top) and uncertainty (middle and bottom) as experimental high fidelity data is gradually added to cokrig low fidelity finite element data.

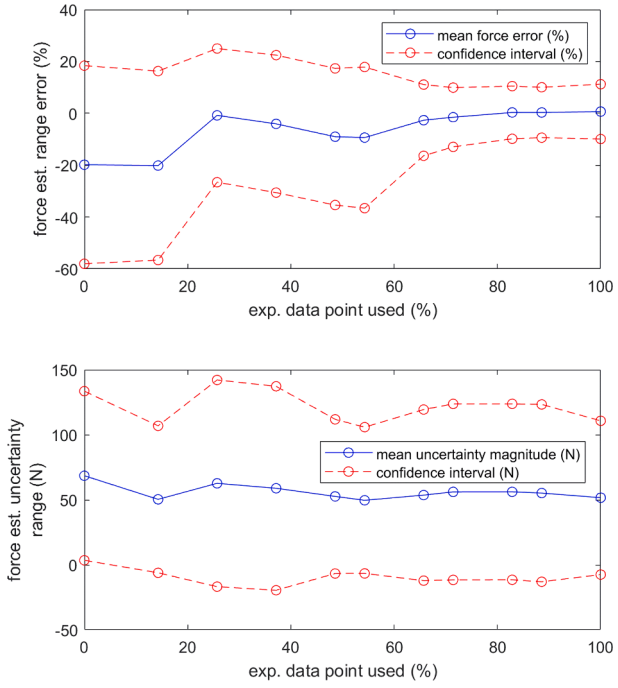

Fig. 13. Change in stiffened panel maximum impact force estimation error (top) and uncertainty (bottom) as experimental high fidelity data is gradually added to cokrig low fidelity finite element data.

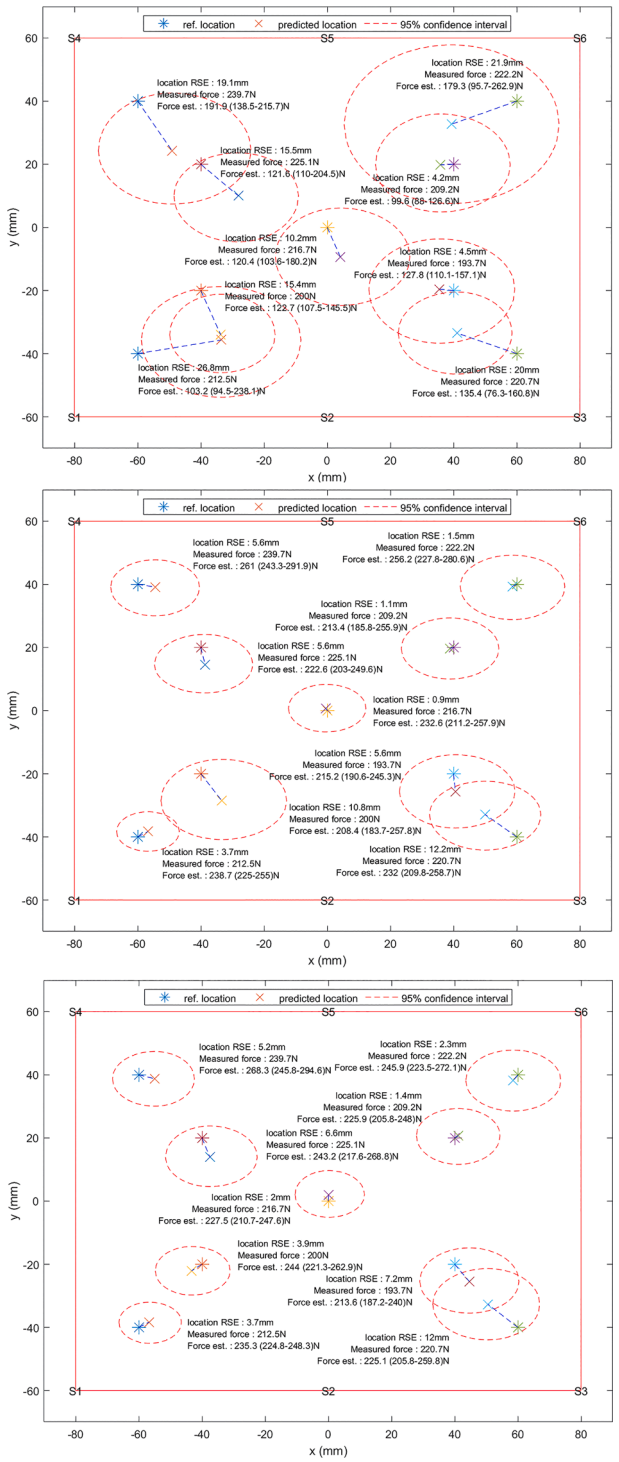

Fig. 14. Impact location and maximum force estimation for plastic impact case (F4) on the flat panel using different reference databases: (top) all FE data, (middle) cokriging with 31.4% experimental samples, (bottom) all experimental data.

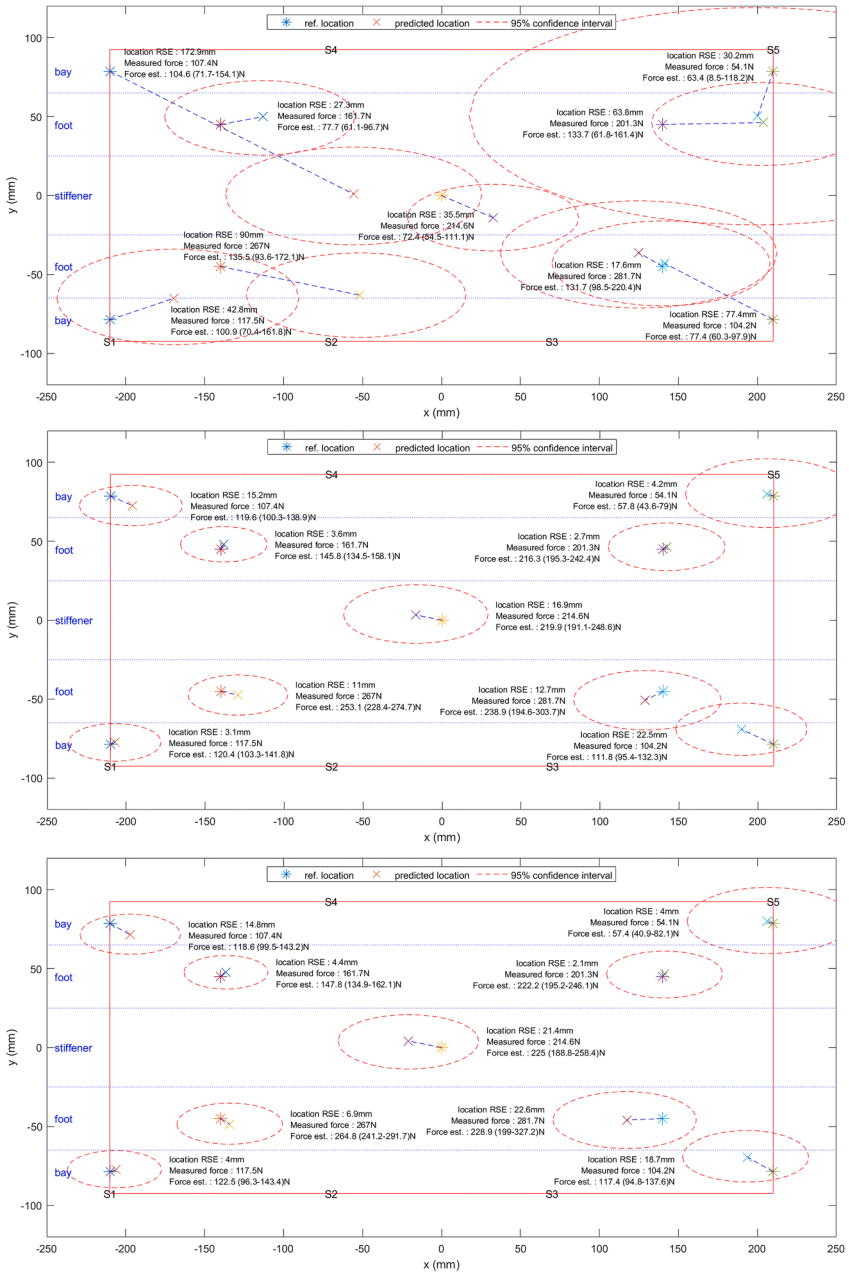

Fig. 15. Impact location and maximum force estimation for reference impact case (S1) on the stiffened panel using different reference databases: (top) all FE data, (middle) cokriging with 65.7% experimental samples, (bottom) all experimental data.

$$F_{max,Rerror} = \begin{cases} \dfrac{(F_{max,range(-)} - F_{max,act})}{F_{max,act}} 100\%, F_{max,act} \leq F_{max,range(-)} \\ 0, F_{max,range(-)} \leq F_{max,Ract} \leq F_{max,range(+)} \\ \dfrac{(F_{max,range(+)} - F_{max,act})}{F_{max,act}} 100\%, F_{max,range(+)} \leq F_{max,Ract} \end{cases} \tag{10}$$

7. Results

Fig. 9 shows the comparison between the maximum impact force gradient (G_{MA}) of sensor 6 on the flat panel for the reference database of the low fidelity FE data and the high fidelity experimental data. It can be seen that there is only a limited correlation

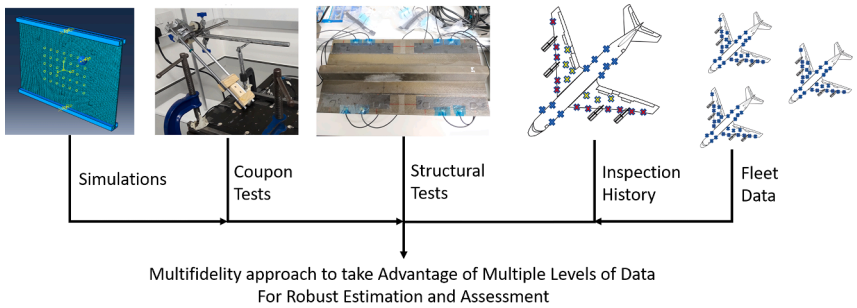

Fig. 16. Possible expansion of multifidelity approach to encompass multiple sources of data.

between the FE and experimental data. Taking some experimental data samples (11 out of 35) and applying cokriging (Fig. 9) shows a significant increase in correlation of the cokriged data with experimental data. This demonstrates how effective the proposed approach can increase the correlation of signal features using a small sample of high fidelity data. This increased correlation should result in improved accuracy for impact location and maximum force estimation.

Fig. 10 and Fig. 11 shows the impact location and maximum force estimation results for the reference case (F1) of the flat panel, using different reference databases with varying amounts of experimental points (maximum is 35 points, 0% indicates full FE data, 100% indicates full experimental data). Here it can be seen that when using only FE data, the error and uncertainty of both location and maximum impact force estimation was very high compared to when using all experimental data. However, when cokriging was applied and experimental samples were gradually added, the error for both location and maximum impact force estimation decreased significantly and started to approach full experimental data error levels starting from 31.4% (11 out of 35 samples) experimental data sample usage, which we take as the optimum percentage (best "cost" to accuracy ratio).

Table 3 shows the errors for both the impact location and maximum force estimation on the flat panel for other test cases (F2 – F6) besides the reference case (F1) for full FE data, full experimental data and optimum percentage of experimental data usage. Here, it can be seen that the accuracy at the optimum percentage was robust for the environmental and operational conditions simulated in the test cases.

Fig. 12 and Fig. 13 shows the impact location and maximum force estimation results for the reference case (S1) of the stiffened panel, using databases with varying amounts of experimental data samples. Similar to the flat panel, with purely FE data, the error and uncertainty was high for both location and maximum impact force estimation. As the amount of experimental data samples was gradually increased, the error for both location and maximum impact force estimation decreased to levels near full experimental data usage at 65.7% experimental data samples (23 out of 35). The uncertainty decreased slightly for the localisation but remained relatively constant for the maximum impact force. This shows how the FE model was less able to capture the behaviour in the stiffened panel compared to the flat panel, most likely due to the added geometrical complexity, and resulted in a higher optimum percentage.

Fig. 14 and Fig. 15 illustrates the comparison between the location and maximum impact force estimation between full FE data and optimum percentage of experimental samples for both flat and stiffened panels. Here it can be seen how at the optimum percentage the accuracy of the estimation is significantly increased compared to using pure FE data.

8. Possible extension of multifidelity approach and future work

Here the mutifidelity approach has been demonstrated to be an effective way to combine different sources of data to achieve reduction of "cost" in constructing a reference database for data driven impact location and maximum impact force estimation methods. Although the example given here is a combination between FE and experimental test data from structural coupons, the cokriging method given here is able to combine data from a wider range of sources, such as tests from different levels of coupon/structure complexity, simulations (e.g. FE), data from similar components, inspection history as well as data from sister/fleet assets (e.g. aircraft, civil structures) as shown in Fig. 16.

By being able to combine data from similar components (e.g. similar geometry panels), it may be possible to reduce the overall amount of data required for a large scale structure. The capability to include inspection history may enable the reference database to become more and more accurate as time goes on and the structure experiences more impacts that are identified through inspection and logged into the reference database. By being able to share the data between sister/fleet assets, it is possible to integrate the operational experience from a large number of assets to obtain a large amount of data.

As mentioned previously in section 5, only the estimate is used from the cokriging results for the reference database. In future studies, it may be possible to take advantage of the variance to construct a stochastic (rather than deterministic) reference database to possibly increase the accuracy of the location and maximum impact force estimates. As seen from the results, the accuracy of the FE simulations has a significant effect on the effectivity of the proposed cokriging method. Although this may pose a significant challenge for larger structures, the proposed method also allows combination of other types of data such as coupon experimental data which can be more realistically collected than experimental data on an operational structure. These considerations will need to be tested on large scale structure to verify the applicability of the proposed method.

9. Conclusion

In this paper a multifidelity approach was shown to reduce the "cost" of constructing the reference database necessary for data driven impact location and severity estimation methods by combining "cheap" FE data with a limited number of "expensive" experimental samples. The results showed that using pure FE data for points used, it was shown that the accuracy increases significantly approaching levels near pure experimental data at only 31.4% and 65.7% of experimental data usage for flat and stiffened composite panel test specimens, signifying a reduction in the need for "expensive" experimental data. Further tests were carried out for impacts under simulated environmental and operational conditions, which showed that the accuracy is robust for the simulated conditions. Thus, by using the proposed approach, it is possible to significantly reduce the "cost" of constructing reference databases with the help of "cheaper" sources of data, thus bringing data driven methods much closer to real life application. The wider context of data fusion is also explored, highlighting the possibility to combine various sources of data (including inspection history as well as data from sister assets) which can possibly be used to create a data driven framework that requires less initial data whilst also being robust and self-improving.

Declaration of Competing Interest

The authors declare that they have no known competing financial interests or personal relationships that could have appeared to influence the work reported in this paper.

Data availability

Data will be made available on request.

Acknowledgement

We would like to express gratitude to the Indonesian Endowment Fund for Education (LPDP) for funding of AHS Ph.D. study.

References

[1] S. Abrate, Impact on composite structures, Cambridge University Press, 2005.
[2] V. Giurgiutiu, Structural health monitoring of aerospace composites, Academic Press, 2015.
[3] Fu H, Seno AH, Khodaei ZS, et al. Design of a Wireless Passive Sensing System for Impact Detection of Aerospace Composite Structures. 2018 5th IEEE Int Workshop Metrol Aerosp MetroAeroSpace [Internet]. Rome, Italy: IEEE; 2018 [cited 2019 Jun 13]. p. 585–589. Available from: https://ieeexplore.ieee.org/document/8453608/.
[4] L. Qiu, X. Lin, Y.u. Wang, S. Yuan, W. Shi, A mechatronic smart skin of flight vehicle structures for impact monitoring of light weight and low-power consumption, Mech. Syst. Sig. Process. 144 (2020) 106829.
[5] Seno, Aliabadi, Impact Localisation in Composite Plates of Different Stiffness Impactors under Simulated Environmental and Operational Conditions, Sensors 19 (17) (2019) 3659.
[6] A.H. Seno, M.H.F. Aliabadi, A novel method for impact force estimation in composite plates under simulated environmental and operational conditions, Smart Mater. Struct. 29 (11) (2020) 115029.
[7] A.H. Seno, Z. Sharif Khodaei, M.H.F. Aliabadi, Passive sensing method for impact localisation in composite plates under simulated environmental and operational conditions, Mech. Syst. Sig. Process. 129 (2019) 20–36.
[8] L. Morse, Z. Sharif Khodaei, M.H. Aliabadi, Reliability based impact localization in composite panels using Bayesian updating and the Kalman filter, Mech. Syst. Sig. Process. 99 (2018) 107–128.
[9] N. Sen, T. Kundu, A new wave front shape-based approach for acoustic source localization in an anisotropic plate without knowing its material properties, Ultrasonics. 87 (2018) 20–32.
[10] M.R. Pearson, M. Eaton, C. Featherston, R. Pullin, K. Holford, Improved acoustic emission source location during fatigue and impact events in metallic and composite structures, Struct. Health Monit. 16 (4) (2017) 382–399.
[11] S. Yin, Z. Cui, J. Fu, T. Kundu, Acoustic source localization in heterogeneous media, Ultrasonics 99 (2019) 105957.
[12] S. Yin, Z. Cui, T. Kundu, Acoustic source localization in anisotropic plates with "Z" shaped sensor clusters, Ultrasonics 84 (2018) 34–37.
[13] G. Sarego, M. Zaccariotto, U. Galvanetto, Artificial neural networks for impact force reconstruction on composite plates and relevant uncertainty propagation, Artif. Neural Netw. (2018) 10.
[14] C.V. Dung, E. Sasaki, Experimental Study on Impact Force Identification Using Output Response of Polyvinylidene Fluoride Sensor, Sens. Mater. 30 (2018) 7–21.
[15] M. Xu, N. Jiang, Dynamic load identification for interval structures under a presupposition of 'being included prior to being measured', App. Math. Model. 85 (2020) 107–123.
[16] Ebrahimkhanlou A, Salamone S. Probabilistic location estimation of acoustic emission sources in isotropic plates with one sensor. In: Kundu T, editor. Portland, Oregon, United States; 2017 [cited 2020 Dec 16]. p. 1017029. Available from: http://proceedings.spiedigitallibrary.org/proceeding.aspx?doi=10.1117/12.2258618.
[17] De simone ME, Ciampa F, Meo M. A hierarchical method for the impact force reconstruction in composites structures. Smart Mater Struct [Internet]. 2018 [cited 2019 May 13]; Available from: http://iopscience.iop.org/article/10.1088/1361-665X/aae11c.
[18] M. Ghajari, Z. Sharif-Khodaei, M.H. Aliabadi, A. Apicella, Identification of impact force for smart composite stiffened panels, Smart Mater. Struct. 22 (8) (2013) 085014.
[19] Z. Sharif-Khodaei, M. Ghajari, M.H. Aliabadi, Determination of impact location on composite stiffened panels, Smart Mater. Struct. 21 (10) (2012) 105026.
[20] P.T. Coverley, W.J. Staszewski, Impact damage location in composite structures using optimized sensor triangulation procedure, Smart Mater. Struct. 12 (5) (2003) 795–803.
[21] A.H. Seno, F.M.H. Aliabadi, A Comparative Study of Impact Localisation in Composite Structures Using Neural Networks under Environmental and Operational Variations, Key Eng. Mater. 827 (2019) 410–415.
[22] E.D. Niri, Determination of the probability zone for acoustic emission source location in cylindrical shell structures, Mech. Syst. Sig. Process. 15 (2015).
[23] E. Dehghan Niri, S. Salamone, A probabilistic framework for acoustic emission source localization in plate-like structures, Smart Mater. Struct. 21 (3) (2012) 035009.
[24] E. Zhang, J. Antoni, P. Feissel, Bayesian force reconstruction with an uncertain model, J. Sound Vib. 331 (4) (2012) 798–814.

[25] E.H. Isaaks, R.M. Srivastava, An Introduction to Applied Geostatistics, Oxford University Press, 1989.
[26] Y. Kuya, K. Takeda, X. Zhang, et al., Multifidelity Surrogate Modeling of Experimental and Computational Aerodynamic Data Sets, AIAA J. 49 (2011) 289–298.
[27] Fernández-Godino MG, Park C, Kim N-H, et al. Review of multi-fidelity models. ArXiv Prepr ArXiv160907196. 2016.
[28] E. Clarkson, Hexcel 8552 IM7 unidirectional prepreg 190 gsm & 35% RC qualification statistical analysis report, Natl. Inst. Aviat. Res. (2012).
[29] Hexcel Composites SA. HexPly® M21 product data sheet. 2010.
[30] L.P P (Physik I. Piezoceramic Materials [Internet]. [cited 2021 Jan 25]. Available from: https://www.pi-usa.us/en/apps-tech/technology/piezo-technology/piezoelectric-materials/.
[31] Abaqus. Abaqus version 6.13 documentation. Dassault Systemes Simulia Corp Providence, RI; 2013.
[32] J. Sirohi, I. Chopra, Fundamental Understanding of Piezoelectric Strain Sensors, J. Intell. Mater. Syst. Struct. 11 (2000) 246–257.
[33] Seno AH, Aliabadi FMH. Uncertainty Quantification for Impact Location and Force Estimation in Composite Structures under Simulated Environmental and Operational Conditions. subm.
[34] CoKriging : algorithm [Internet]. [cited 2020 Nov 30]. Available from: http://spatial-analyst.net/ILWIS/htm/ilwisapp/cokriging_algorithm.htm.